

# Magnetophotoselection Study of the Lowest Excited Triplet State of the Primary Donor in Photosynthetic Bacteria

Igor V. Borovykh,<sup>†</sup> Ivan I. Proskuryakov,<sup>†,‡</sup> Irina B. Klenina,<sup>§</sup> Peter Gast,<sup>†</sup> and Arnold J. Hoff<sup>\*,†</sup>

Department of Biophysics, Huygens Laboratory, P.O. Box 9504, 2300 RA Leiden, The Netherlands, and  
Institute of Basic Biological Problems RAS, Pushchino, 142292, Russia

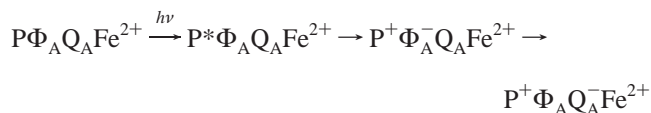
Received: October 25, 1999; In Final Form: January 25, 2000

The first time-resolved magnetophotoselection study of the primary donor triplet state (<sup>3</sup>P) in bacterial reaction centers from *Rhodobacter sphaeroides* R26 and *Rhodospseudomonas viridis* is reported. With direct excitation of the primary donor, this approach provides the orientation (spherical coordinates  $\delta$ , colatitude, and  $\gamma$ , longitude) of the excited optical transition moment in the principal triplet axis system. It is essentially free from the effects of spin–lattice relaxation of <sup>3</sup>P, enabling magnetophotoselection measurements over a wide temperature range. Two independently measured triplet-state spectra, excited with light polarized parallel and perpendicular to the EPR magnetic field, are simulated with the same set of parameters. This procedure results in a high precision (ca.  $\pm 5^\circ$  with sufficient signal/noise ratio) of the obtained spherical coordinates of the optical transition moment vector. We find  $\delta = 80 \pm 5^\circ$ ,  $\gamma = 70 \pm 5^\circ$  and  $\delta = 75 \pm 5^\circ$ ,  $\gamma = 70 \pm 5^\circ$  for *Rb. sphaeroides* R26 and *Rps. viridis*, respectively. We demonstrate that excitation of the sample with nonpolarized light is essentially nonisotropic. Neglect of this effect in spectral simulations of light-induced signals may lead to considerable error in the parameters determined.

## Introduction

Resolution of the structure of photosynthetic bacterial reaction centers (RCs)<sup>1</sup> stimulated hopes that it would lead to ultimate understanding of the function of these energy-transducing pigment–protein complexes. After more than a decade of research, however, these hopes are still not met. Moreover, evidence is accumulating that the RC structure should not be considered as fixed, but as a variable structure that depends on the functional state of the reaction center.<sup>2</sup> It is therefore of great interest to study the structure–function relationships for RCs in states other than the ground state. EPR spectroscopy of the triplet state provides a useful technique for such an approach.

In bacterial photosynthesis, excitation of the reaction center triggers a sequence of fast electron-transfer reactions, which proceed along one of the two pseudosymmetric cofactor chains (A-branch).<sup>3</sup> Primary charge separation may be summarized as follows:



where P denotes the primary donor, a dimer of bacteriochlorophyll (BChl) molecules,  $\Phi_{\text{A}}$  is the intermediary electron acceptor, a bacteriopheophytin, and  $\text{Q}_{\text{A}}$  is the first acceptor quinone complexed to a high-spin  $\text{Fe}^{2+}$  ion. The triplet state of P (<sup>3</sup>P) is populated when forward electron transfer past acceptor  $\Phi_{\text{A}}$  is blocked by removing  $\text{Q}_{\text{A}}$  or by its prereduction, thereby

increasing the lifetime of the primary radical pair (RP)  $\text{P}^+\Phi_{\text{A}}^-$ . The EPR spectrum of <sup>3</sup>P is characterized by its unique electron spin polarization (ESP), i.e., the nonequilibrium population of the triplet spin sublevels. It was explained<sup>4</sup> by mixing of the singlet (S) and T<sub>0</sub> triplet state of the RP (S–T<sub>0</sub> mechanism of spin evolution) followed by recombination with selective population of the T<sub>0</sub> sublevel of <sup>3</sup>P. The triplet-state formation is an energy-dissipating channel, and its study would seem not to directly give insight into the energy-transducing forward electron transfer. However, the triplet resides on the same BChl molecules that are involved in the functional electron-transfer process, and EPR spectroscopy of <sup>3</sup>P has contributed considerably to the elucidation of the dimeric structure of the primary donor of bacterial photosynthesis<sup>5</sup> prior to crystallographic structure determination. EPR spectroscopy indicated localization of the triplet state on a monomeric pigment in reaction centers of plant photosystems I and II,<sup>3,5</sup> and also played a decisive role in establishing the presence of radical pair states in the primary charge-transfer processes.<sup>4</sup> Magnetophotoselection measurements provide additional information on the properties of the triplet state, and therefore on the structure of P.

Magnetophotoselection (MPS) combines optical photoselection with electron paramagnetic resonance.<sup>6</sup> When a nonoriented EPR sample is illuminated with light polarized with its electric vector either parallel or perpendicular to the magnetic field, different subpopulations of molecules are excited depending on the polarization of the  $\text{S}_1 \leftarrow \text{S}_0$  transition (orientation of the optical transition moment in the molecular frame). Therefore, the shape of the EPR spectrum of a magnetically anisotropic species will be directly related to the fraction of polarization of the optical transition projected on each molecular axis. Quantita-

<sup>†</sup> Huygens Laboratory.

<sup>‡</sup> On leave from the Institute of Basic Biological Problems RAS, Pushchino.

<sup>§</sup> Institute of Basic Biological Problems RAS.

tive analysis of MPS spectra provides the orientation of the excited optical transition moment vector in the triplet principal axis system.

The  $^3\text{P}$  EPR spectrum is strongly anisotropic, mostly because of the spin–spin dipolar interaction between the unpaired electrons.<sup>5</sup> This makes  $^3\text{P}$  suitable for MPS studies. Magneto-photoselection measurements of  $^3\text{P}$  in photosynthetic bacterial preparations were first reported in ref 7. Further studies resulted in the determination of the relative orientation of the  $^3\text{P}$  magnetic axes, and the  $\text{P}$  and  $\Phi$  transition moments in *Rhodobacter sphaeroides* R26 reaction centers.<sup>8</sup> Later, MPS with excitation into the  $\text{Q}_\text{X}$  optical bands of  $\text{P}$  and  $\Phi$  was studied,<sup>9</sup> and the reaction center absorption spectrum in the 520–660 nm region was analyzed. Another study was aimed at the determination of the relative orientations of the optical and magnetic axes of  $\text{P}$  and a carotenoid molecule in wild-type *Rb. sphaeroides* RCs and chromatophores.<sup>10</sup> At the time when the X-ray structure of the reaction centers was not available, these measurements provided insight into the arrangement of electron-transfer cofactors of the RCs. Recent MPS measurements of D1–D2–cyt *b559* RC complexes of photosystem (PS) II<sup>11</sup> yielded a molecular model of the primary donor in a system whose crystal structure remains to be elucidated.<sup>12</sup>

Previously, for MPS measurements, conventional EPR with field modulation and lock-in detection was generally used. We are aware of only a few studies<sup>13</sup> where time-resolved EPR was used in conjunction with MPS to investigate nonphotosynthetic systems, mostly aromatic molecules in frozen solutions. The important advantage of the time-resolved EPR experiment is that it enables detection of the initial spin polarization of the signal, before significant spin–lattice relaxation or triplet depopulation develops. In contrast, the spectra obtained with conventional EPR are essentially steady-state spectra; thus, their shape depends on the kinetic properties of the paramagnetic species under study. For spectral simulation and fitting, the corresponding rate constants (which are often not accurately known) have to be introduced into the data treatment procedure, decreasing the reliability of information obtained from MPS. In certain cases (for example,  $^3\text{P680}$ , the primary donor of PSII), cw-EPR study is limited to very low temperatures because of fast relaxation.<sup>14</sup>

In the present work we utilized the direct detection EPR (DDEPR) technique.<sup>14–16</sup> Its high time resolution (ca. 50 ns) allows detection of signals shortly after the exciting laser flash, before any significant relaxation between triplet spin sublevels has taken place. We report a study of  $^3\text{P}$  EPR spectra in several RC preparations of *Rb. sphaeroides* R26 and in *Rhodospseudomonas viridis* RCs in the temperature range from 4 to 50 K. The observed spin-polarized DDEPR spectra of  $^3\text{P}$  show strong photoselection effects. The photoselected spectra can be very well simulated, yielding quite accurate information on the orientation of the optical transition dipole  $\text{Q}_\text{Y}$  of  $\text{P}$  in the  $^3\text{P}$  magnetic axis system. Additionally, we show that excitation of a sample in an EPR cavity is nonisotropic, even with unpolarized light. Preliminary results of the present work have been reported.<sup>17</sup>

## Experimental Section

**Biochemical Procedures.** Photoselected EPR spectra of  $^3\text{P}$  were measured for three different RC preparations from *Rb. sphaeroides* R26 and one from *Rps. viridis*. RCs of *Rb. sphaeroides* R26 were isolated as described by Feher et al.<sup>18</sup> Replacement of the non-heme high-spin  $\text{Fe}^{2+}$  by diamagnetic  $\text{Zn}^{2+}$  (Zn substitution) was performed as described by Tiede et

al.<sup>19</sup> Removal of  $\text{Q}_\text{A}$  (quinone depletion; >95%) was carried out according to Okamura et al.<sup>20</sup> RCs of *Rps. viridis* were isolated as described by Den Blanken et al.<sup>21</sup>

Quinone-depleted RCs of *Rb. sphaeroides* R26 were frozen in the dark. Nontreated and Zn-substituted RCs of *Rb. sphaeroides* R26 and RCs of *Rps. viridis* were frozen under light in the presence of 10 mM sodium ascorbate to prereduce  $\text{Q}_\text{A}$ . All EPR samples contained 66% (v/v) glycerol and were prepared in 3 mm i.d. quartz tubes. The final optical density of the samples was 10–15  $\text{cm}^{-1}$  in the primary donor absorption band. The samples were degassed by three freeze–pump–thaw cycles and sealed under vacuum. This procedure decreased the probability of crack formation when the samples were being frozen. No evidence of  $\Phi_\text{A}^-$  accumulation in *Rps. viridis* samples was found, most likely because of the low light intensities applied.

**Instrumental Details.** As an excitation light source, a Continuum Surelight I-pumped OPO laser was used with flash duration of ca. 4 ns and an output power of about 3 mJ. The incident power was attenuated to ca. 0.1  $\text{mJ}\cdot\text{cm}^{-2}$  at the sample surface inside the EPR cavity to avoid light saturation of the magnetophotoselection effects. Samples were excited into the near-infrared absorption band of the primary donor, around 900 nm for RCs of *Rb. sphaeroides* R26 and around 980 nm for *Rps. viridis*, corresponding to the respective  $\text{Q}_\text{Y}$ -transitions of  $\text{P}$  at low temperature.<sup>22</sup> The excitation bandwidth was 4–5 nm. The OPO light is 95% vertically plane-polarized. To provide control of the polarization plane, a system of a depolarizing light guide followed by a Glan-Thompson prism was used. Rotation of the prism produced excitation light with an adjustable angle between its electric vector and the EPR magnetic field. The flash intensity variation was only 2% when the polarization plane was rotated, and the same spot of the sample was illuminated at any angle. These properties of the polarizing system were important for quantitative data treatment. For depolarized excitation, the prism was removed.

An important factor in the MPS measurements is a possible partial light depolarization while passing quartz parts of the cryostat and the sample tube. To estimate the degree of such depolarization, a special experiment was designed. A piece of polarizing film was attached to the face of a small phototransistor (Siemens BPX 81), which could be fitted inside the EPR sample tube. The beam of a dc-powered lamp after passing an appropriate interference filter and a Glan-Thompson prism was directed onto the transistor, and the dependence of the photocurrent on the rotation angle of the prism was studied. If the cryostat and/or EPR tube cause depolarization, oscillatory patterns obtained with the transistor inserted into the EPR tube and/or the cryostat would differ from those of the transistor alone. Induced depolarization will cause a decrease in the amplitude of the sinusoidal pattern, and a shift of its baseline to higher values. It was observed that up to 545 nm (the shortest wavelength used) neither the sample tube nor the cryostat induced measurable depolarization (<1%, achieved accuracy).

DDEPR experiments were performed as described earlier.<sup>14,15</sup> In short, a home-built X-band EPR spectrometer was used, equipped with a Varian rectangular TE<sub>102</sub> optical transmission cavity. A laser pulse initiated a reaction producing paramagnetic states. Following the flash, a boxcar sampled the changes in microwave power reflected from the cavity. For obtaining transient EPR spectra, the sampling gate width of 1.3  $\mu\text{s}$  and its delay of 0.2  $\mu\text{s}$  after the flash were fixed, and the magnetic field was slowly swept while the output signal of the boxcar was recorded. In the DDEPR experiment the signal appeared in direct absorption and emission mode. The overall time

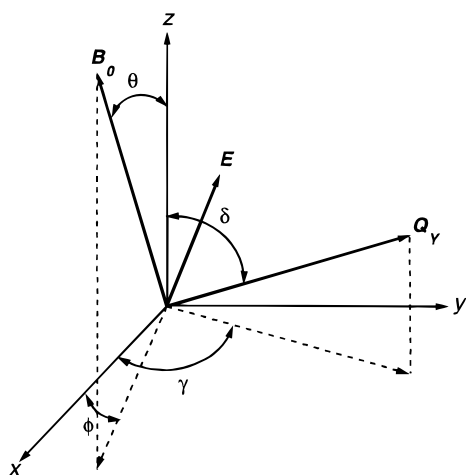


**Figure 1.** Axis system and vectors involved in the simulation of the MPS  $^3\text{P}$  spectra shown for the case of  $\mathbf{E} \perp \mathbf{B}_0$ .  $x$ ,  $y$ ,  $z$ ;  $^3\text{P}$  principal magnetic axes (axes of its zero-field splitting tensor);  $\mathbf{Q}_Y$ , excited optical transition moment;  $\mathbf{E}$ , excitation light electric vector;  $\mathbf{B}_0$ , magnetic field vector.

resolution of our setup was about 50 ns. The temperature in the Oxford Instruments helium gas-flow cryostat was regulated with a home-built temperature controller, which could be set with 1 K accuracy, and stabilized the temperature to  $\pm 0.2$  K.

**Spectral Simulations.** For nonphotoselected spectral simulations we utilized the standard procedure.<sup>23</sup> Photoselection effects were accounted for by introducing intensity coefficients for each orientation of  $^3\text{P}$  in the magnetic field, equal to the cosine square of the angle between the  $\mathbf{Q}_Y$  and the electric vector  $\mathbf{E}$  of the excitation light.<sup>24</sup> The procedure for simulation of the MPS spectra is as follows. The first simulation step is to calculate the so-called “isotropic” spectrum constructed by the summation of one  $\mathbf{E} \parallel \mathbf{B}_0$  spectrum and two  $\mathbf{E} \perp \mathbf{B}_0$  spectra. Here the  $\mathbf{E} \parallel \mathbf{B}_0$  ( $\mathbf{E} \perp \mathbf{B}_0$ ) spectra are the experimental spectra obtained under excitation by plane-polarized light with its electric vector parallel (perpendicular) to the constant magnetic field of the spectrometer. The isotropic spectrum corresponds to the case of equal excitation probability of any orientation of  $\text{P}$  and is independent of the orientation of  $\mathbf{Q}_Y$  in the  $^3\text{P}$  axis frame. From the simulation of the isotropic spectrum, the zero-field splitting (ZFS) parameters, the homogeneous line widths, and the principal  $\mathbf{g}$  tensor values of  $^3\text{P}$  are obtained, considered further as constants. In the second step, the  $\mathbf{E} \parallel \mathbf{B}_0$  and  $\mathbf{E} \perp \mathbf{B}_0$  spectra are simulated. The intensity coefficients for the two orthogonal orientations of  $\mathbf{E}$  relative to  $\mathbf{B}_0$  averaged over all orientations of  $^3\text{P}$  relative to the electric vector  $\mathbf{E}$  (with its  $\theta$  and  $\phi$  coordinates fixed) are, for  $\mathbf{E} \parallel \mathbf{B}_0$

$$\langle \cos^2(\mathbf{E}, \mathbf{Q}_Y) \rangle = [\sin \theta \cos \phi \sin \delta \cos \gamma + \sin \theta \sin \phi \sin \delta \sin \gamma + \cos \theta \cos \delta]^2 \quad (\text{A})$$

and for  $\mathbf{E} \perp \mathbf{B}_0$

$$\langle \cos^2(\mathbf{E}, \mathbf{Q}_Y) \rangle = (1/2)[(\cos \theta \cos \phi \sin \delta \cos \gamma + \cos \theta \sin \phi \sin \delta \sin \gamma - \sin \theta \cos \delta)^2 + (\sin \phi \sin \delta \cos \gamma - \cos \phi \sin \delta \sin \gamma)^2] \quad (\text{B})$$

with the angles denoted in Figure 1 and the angular brackets standing for averaging. This simulation step provides the orientation of the optical transition moment,  $\mathbf{Q}_Y$ , (angles  $\delta$  and  $\gamma$ ) in the  $^3\text{P}$  magnetic axis system. Because we simulate two independently measured spectra of very different shapes with

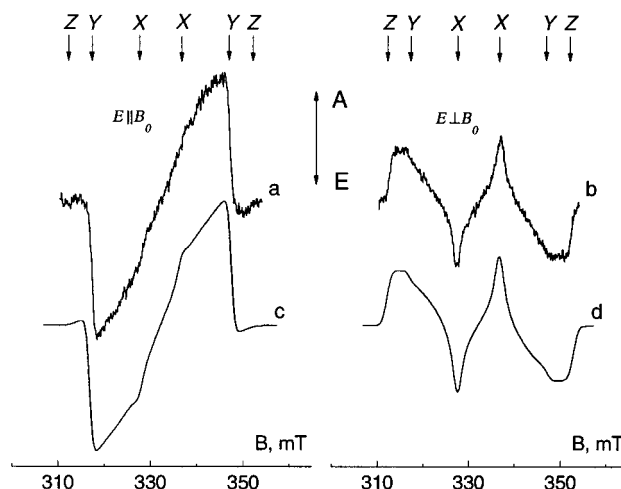


**Figure 2.** Experimental (a, b) and calculated (c, d)  $^3\text{P}$  spectra for *Rb. sphaeroides* R26 RCs with reduced  $Q_A$  for the polarization plane of the excitation light parallel (a, c) and perpendicular (b, d) to the magnetic field  $\mathbf{B}_0$ . Experimental conditions:  $T = 10$  K,  $\lambda_{\text{exc}} = 900$  nm. Note that the signal amplitudes have not been normalized.  $X$ ,  $Y$ , and  $Z$  are the EPR transitions for which the  $x$ ,  $y$ , and  $z$  magnetic axes of  $^3\text{P}$  are parallel to the magnetic field  $\mathbf{B}_0$ .  $A$  and  $E$  stand for absorption and emission of microwaves.

the same set of angular parameters, the error of the determination of the angles is quite low (ca.  $\pm 5^\circ$  with sufficient signal/noise ratio). It is important to note that not only the correspondence to the spectral shape but also the relative amplitudes of the two experimental spectra are used as a fit quality criterion.

## Results and Discussion

**RCs of *Rb. sphaeroides* R26.** Figure 2 shows the DDEPR spectra of  $^3\text{P}$  in a sample of *Rb. sphaeroides* R26 RCs with reduced  $Q_A$ , excited with light polarized parallel (a) and perpendicular (b) to the magnetic field of the spectrometer. The difference between the two spectra is the result of MPS. Even without spectral simulations the changes induced by the rotation of the polarization plane can be understood qualitatively. When light is polarized parallel to the magnetic field, we predominantly excite the molecules of  $\text{P}$  with  $\mathbf{Q}_Y$  parallel to the magnetic field. From LD-ADMR<sup>25</sup> it is known that the angle between  $\mathbf{Q}_Y$  and the triplet  $y$  axis is small, so RCs with the  $y$  triplet axis parallel to the magnetic field have higher excitation probability. In fact, the  $\mathbf{E} \parallel \mathbf{B}_0$  spectrum (Figure 2a) demonstrates increased contribution of the  $Y$  canonical peaks.

Spectral simulation provides quantitative information. Fitting of the isotropic spectrum constructed from the spectra of Figure 2a,b gives the following values: ZFS parameters,  $D = 0.0188 \pm 0.0003 \text{ cm}^{-1}$  and  $E = 0.0032 \pm 0.0003 \text{ cm}^{-1}$ , the isotropic homogeneous line width,  $\Delta B = 1.3 \text{ mT}$ , and principal  $\mathbf{g}$  tensor values of  $^3\text{P}$ ,  $g_X = g_Y = 2.002 \pm 0.001$ ,  $g_Z = 2.000 \pm 0.001$ . The  $g$  values agree with those determined earlier at 15 K.<sup>26</sup> The value of  $g_Z$  lies below that of the free electron, which is probably a manifestation of nonnegligible spin-orbit coupling in the triplet state. The ZFS parameters coincide with their literature values.<sup>27</sup> As described in the Experimental Section, these parameters were then included in the simulation procedure of the  $\mathbf{E} \parallel \mathbf{B}_0$  and  $\mathbf{E} \perp \mathbf{B}_0$  spectra, with spherical coordinates  $\delta$  and  $\gamma$  (see Figure 1) as fit parameters. Best fits shown in Figure 2c,d were obtained with the values  $\delta = 80 \pm 5^\circ$  and  $\gamma = 70 \pm 5^\circ$ . These angles are close to those determined earlier from LD-ADMR measurements at 1.5 K,  $\delta = 74 \pm 5^\circ$  and  $\gamma = 85 \pm$



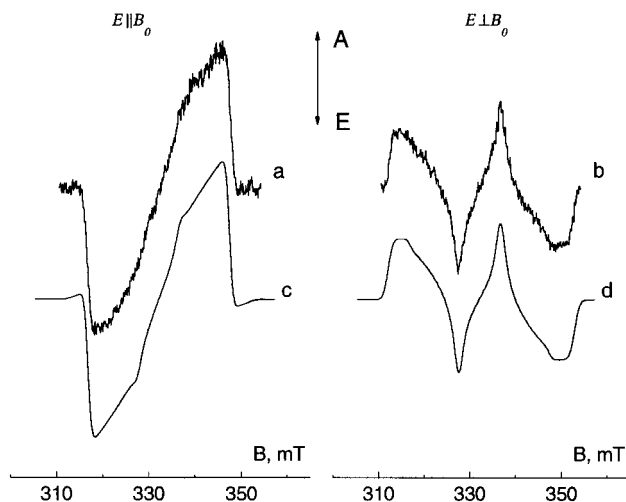


**Figure 3.** Experimental (a, b) and calculated (c, d)  $^3\text{P}$  spectra for *Rb. sphaeroides* R26 RCs with removed  $\text{Q}_\text{A}$  for  $\text{E}||\text{B}_0$  (a, c) and  $\text{E}\perp\text{B}_0$  (b, d). Experimental conditions are the same as in Figure 2.

$5^\circ$ .<sup>25</sup> Somewhat different values of the spherical coordinates of  $\text{Q}_\text{Y}$  were reported in our preliminary communication.<sup>17</sup> In that work rather high light intensities were used, leading to partial light saturation of the MPS effects. In the present work much lower light intensities were applied, providing more accurate determination of  $\delta$  and  $\gamma$ .

An important factor which may severely affect the precision of the angle determination is possible  $^3\text{P}$  excitation with depolarized light. Before reaching the sample, the laser beam passes through the quartz parts of the cryostat and the sample tube, and then propagates within the sample itself. As discussed in the Experimental Section, passing through the cryostat and sample tube does not cause measurable depolarization. To estimate the effect of light depolarization inside the sample, model simulations were carried out in which different levels of depolarized light were allowed for, and the resulting spectra were fitted to the experimental ones by varying  $\delta$  and  $\gamma$ . It was found that such fitting was only possible if the fraction of depolarized excitation did not exceed 5% of the polarized light, resulting in a  $10^\circ$  increase of  $\delta$ . As this maximally allowed deviation brings the angle outside the range of its LD-ADMR value (determined with  $5^\circ$  accuracy<sup>25</sup>), we conclude that the effect of light depolarization inside the sample is appreciably smaller than 5%. This conclusion seems to be justified by the observation that, for the high optical densities used, excitation light is absorbed mainly on the surface of the sample, before any depolarization takes place. In further simulations, therefore, depolarization of excitation light was neglected.

Utilizing the orientation of the  $^3\text{P}$  axes relative to the crystallographic axes determined earlier,<sup>29</sup> one may calculate the  $\text{Q}_\text{Y}$  orientation relative to the molecular frame of the pigments. Such recalculation provides the  $\text{Q}_\text{Y}$  spherical coordinates  $\delta' = 78^\circ$  and  $\gamma' = 71^\circ$ , now in the average crystallographic axes of the primary donor dimer, as described in ref 29. The structure of the *Rb. sphaeroides* R26 RCs is close to  $\text{C}_2$ -symmetric relative to the axis connecting the center of the primary donor and the non-heme iron atom.<sup>1,3,28</sup> If P were perfectly  $\text{C}_2$ -symmetric,  $\delta' = 90^\circ$  would be expected. The deviation from this value confirms the conclusion<sup>29,30</sup> that the structure of the primary donor is not perfectly  $\text{C}_2$ -symmetric, also with respect to the  $\text{Q}_\text{Y}$  orientation.

The EPR spectra of  $^3\text{P}$  in  $\text{Q}_\text{A}$ -depleted RCs of *Rb. sphaeroides* (Figure 3a,b) are similar to the spectra of RCs with reduced primary acceptor described above. The isotropic spectrum is

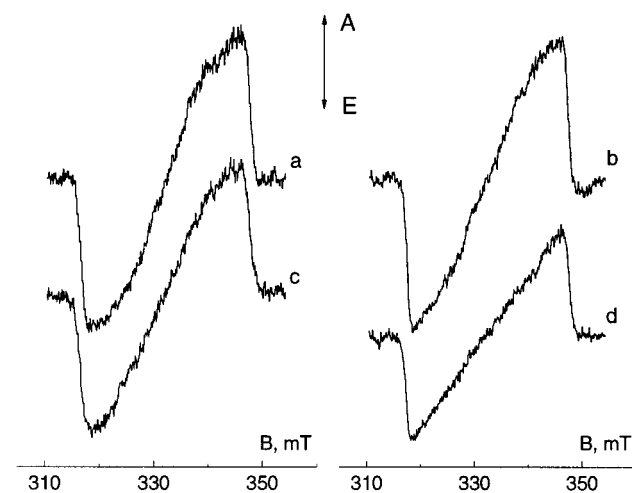


**Figure 4.**  $^3\text{P}$  spectra generated by laser light with the electric vector parallel to the magnetic field in  $\text{Q}_\text{A}$ -depleted (a, c) and  $\text{Q}_\text{A}$ -reduced (b, d) RCs of *Rb. sphaeroides* R26 at 10 K (a, b) and 50 K (c, d).

well simulated with the same set of parameters as for the  $\text{Q}_\text{A}$ -reduced preparation (data not shown). Best fits of the  $\text{E}||\text{B}_0$  and  $\text{E}\perp\text{B}_0$  spectra (Figure 3c,d) are obtained with  $\delta = 90 \pm 5^\circ$  and  $\gamma = 70 \pm 5^\circ$ , only slightly different from the angles for  $\text{Q}_\text{A}$ -reduced RCs. On one hand, this means that the rather harsh biochemical procedure that was used for  $\text{Q}_\text{A}$  removal and the presence of a negative charge on  $\text{Q}_\text{A}$  do not drastically change the properties of  $^3\text{P}$ . On the other hand, the  $^3\text{P}$  MPS spectra in the two preparations are not entirely identical, indicating that the  $\text{Q}_\text{A}$  depletion procedure does have some effect on the primary donor. A similar conclusion was reached earlier from the observed correlation of the P absorption band shift and the amount of quinone in the RC.<sup>31</sup>

**Temperature Dependence.** In the range between 10 and 50 K no temperature dependence of the spin-polarized  $^3\text{P}$  signal in  $\text{Q}_\text{A}$ -depleted RCs of *Rb. sphaeroides* R26 is observed. This is illustrated in Figure 4a,c for the  $\text{E}||\text{B}_0$  spectra. The triplet state spectra in  $\text{Q}_\text{A}$ -reduced RCs, however, do change significantly. Apart from the distortion of the  $\text{E}||\text{B}_0$  spectra shown in Figure 4b,d, the amplitude ratio of the  $\text{E}\perp\text{B}_0$  to the  $\text{E}||\text{B}_0$  spectra drops considerably with increased temperature (data not shown). The described temperature-induced changes are to a large extent completed at 30 K. These changes cannot be simulated within the MPS model; thus, they are not induced purely by rotation of  $\text{Q}_\text{Y}$  relative to the  $^3\text{P}$  magnetic axes. To exclude possible effects of spin–lattice relaxation or depopulation of  $^3\text{P}$  on the shape of its spin-polarized EPR signal, control measurements were performed. It was checked that there was no change in the shape of the spectrum when the duration of the sampling boxcar gate or its delay after excitation flash was varied between 0.2 and 1.5  $\mu\text{s}$ . Thus, the observed temperature-induced effects must be attributed to a change in the initial spin polarization of  $^3\text{P}$ . The most probable cause of the observed temperature effect is the influence of fast spin–lattice relaxation of the reduced iron–quinone complex  $\text{Q}_\text{A}^-\text{Fe}^{2+}$  on the primary radical pair via the exchange interaction between  $\Phi_\text{A}^-$  and  $\text{Q}_\text{A}^-$ .<sup>32</sup> One important consequence of such interaction is the induced deviation from selective  $\text{S}-\text{T}_0$  population of  $^3\text{P}$ , which changes the shape of the spin-polarized  $^3\text{P}$  signal.<sup>33</sup> The spin–lattice relaxation of  $\text{Q}_\text{A}^-\text{Fe}^{2+}$  is known<sup>34</sup> to increase rapidly in the same temperature range for which the major effects on the shape of the spin-polarized  $^3\text{P}$  signal develop (Figure 4b,d). For the simulation of spin-polarized  $^3\text{P}$  spectra with  $\text{S}-\text{T}_{\pm 1}$  contribution, one may employ the models that consider a system of three S

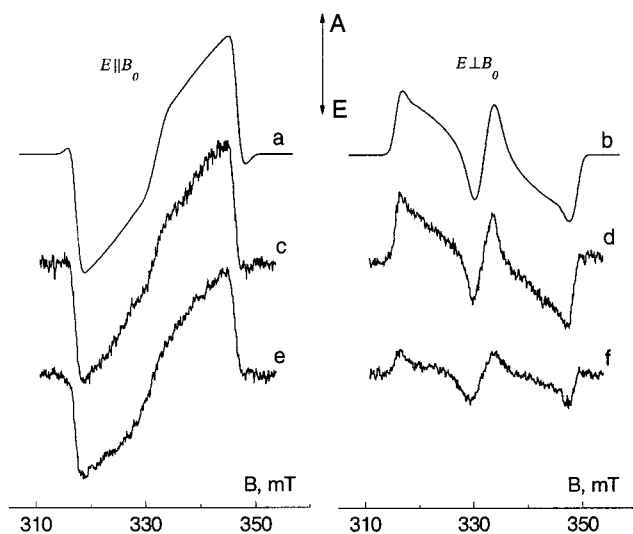


**Figure 5.**  $^3\text{P}$  spectra in *Rps. viridis*  $\text{Q}_\text{A}$ -reduced RCs with  $\text{E}||\text{B}_0$  (a, c, e) and  $\text{E}\perp\text{B}_0$  (b, d, f). Experimental conditions:  $\lambda_\text{exc} = 980$  nm,  $T = 6$  K (c, d), and  $T = 30$  K (e, f). (a) and (b) are calculated spectra; note that to reach correspondence with the recorded spectrum (c) the amplitude of the  $\text{E}||\text{B}_0$  spectrum (a) was multiplied by 1.39.

$= 1/2$  spins for describing changes of the steady-state polarization of  $^3\text{P}$  in *Rps. viridis* RCs at temperatures above 20 K.<sup>32,33</sup>

If the  $\text{Fe}^{2+}$  ion is replaced by diamagnetic  $\text{Zn}^{2+}$ , the above-described temperature dependence disappears (data not shown), and the spectra at any temperature in the considered range remain similar to that of the  $\text{Q}_\text{A}$ -depleted preparation. The values of the ZFS parameters, line width, and principal  $\mathbf{g}$  tensor components of  $^3\text{P}$ , and spherical coordinates of  $\mathbf{Q}_\text{Y}$  in Zn-substituted *Rb. sphaeroides* RCs are then the same as those determined for  $\text{Q}_\text{A}$ -reduced samples at 10 K. The absence of temperature-induced  $\mathbf{Q}_\text{Y}$  rotation in Zn-substituted and  $\text{Q}_\text{A}$ -depleted RCs of *Rb. sphaeroides* R26 shows that in the range 10–50 K the triplet is localized on the primary donor molecule. We conclude that up to 50 K there is no triplet hopping to the adjacent monomeric BChl molecule, as was proposed earlier<sup>35</sup> to explain the temperature dependence of the ZFS parameter  $D$ , for such hopping would change the effective  $\mathbf{Q}_\text{Y}$  orientation. The values of  $\delta$  and  $\gamma$  correspond to the case of triplet delocalization between the two halves of the P dimer, as discussed in ref 29.

**RCs of *Rps. viridis*.** The magnetic interaction between the  $\text{Q}_\text{A}^-\text{Fe}^{2+}$  complex and the reduced intermediary acceptor  $\Phi_\text{A}^-$  in the RCs of *Rps. viridis* is known to be about 2 orders of magnitude larger than that in *Rb. sphaeroides* R26.<sup>36</sup> It is therefore of interest to compare MPS of *Rps. viridis* RCs with that of  $\text{Q}_\text{A}$ -reduced RCs of *Rb. sphaeroides*. Figure 5c,d shows the  $\text{E}||\text{B}_0$  and  $\text{E}\perp\text{B}_0$  spin-polarized spectra of  $^3\text{P}$  in  $\text{Q}_\text{A}$ -reduced RCs of *Rps. viridis* at 6 K. The spectra are temperature-independent between 4 and 6 K. In contrast with the data presented so far, for *Rps. viridis* even the low-temperature spectra of  $^3\text{P}$  cannot be explicitly simulated within the adopted model. If, however, an independent amplitude normalization of the spectra calculated for  $\text{E}||\text{B}_0$  and  $\text{E}\perp\text{B}_0$  is allowed for, a near-perfect fit is achieved. Curves a and b of Figure 5 present such fits obtained when the amplitude of the calculated  $\text{E}||\text{B}_0$  spectrum is additionally multiplied by 1.39. The spectra were calculated for the literature values<sup>27</sup> of the ZFS parameters  $D = 0.0156$   $\text{cm}^{-1}$  and  $E = 0.0040$   $\text{cm}^{-1}$  and spherical coordinates  $\delta = 75 \pm 5^\circ$  and  $\gamma = 70 \pm 5^\circ$ , not significantly different from the angles found for *Rb. sphaeroides* with reduced  $\text{Q}_\text{A}$ . Apparently, the less symmetric triplet delocalization over the two

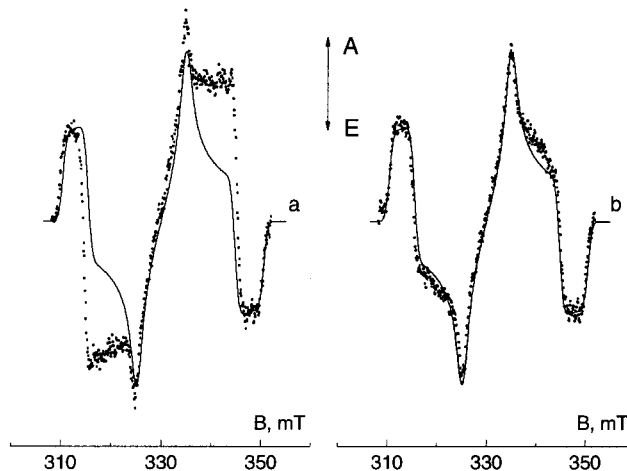


**Figure 6.** Dots, spectra of the  $^3\text{P}$  state obtained in  $\text{Q}_\text{A}$ -reduced *Rb. sphaeroides* R26 RCs with depolarized light (a) and constructed by summation of one  $\text{E}||\text{B}_0$  with two  $\text{E}\perp\text{B}_0$  spectra (b). The solid line shows the calculated spectrum of isotropically excited  $^3\text{P}$ , which is normalized to fit the amplitudes of the Z components of the corresponding experimental spectra. Experimental conditions are as in Figure 2.

halves of the primary donor dimer in *Rps. viridis* RCs compared to  $^3\text{P}$  of *Rb. sphaeroides* R26<sup>29</sup> has little effect on the configuration of  $\mathbf{Q}_\text{Y}$  and the triplet  $z$  axis.

The most probable reason for the apparent amplitude discrepancy between the  $\text{E}\perp\text{B}_0$  and  $\text{E}||\text{B}_0$  spectra is the above-mentioned strong interaction between the  $\text{Q}_\text{A}^-\text{Fe}^{2+}$  acceptor complex and the primary radical pair. As a consequence, spin evolution in the  $\text{P}^+\Phi_\text{A}^-$  RP can no longer be considered apart from the third effective  $S = 1/2$  spin of the  $\text{Q}_\text{A}^-\text{Fe}^{2+}$  complex, and the initial population of the  $^3\text{P}$  spin sublevels deviates from pure  $T_0$  even at low temperatures in the absence of fast spin–lattice relaxation of the iron–quinone complex.<sup>33</sup> At  $T \geq 10$  K the line shape of the *Rps. viridis*  $^3\text{P}$  EPR spectrum undergoes rapid change, especially that of the  $\text{E}\perp\text{B}_0$  spectrum, the relative amplitude of which drops considerably (illustrated in Figure 5e,f for  $T = 30$  K). We ascribe this temperature dependence to the buildup of relaxation in the  $\text{Q}_\text{A}^-\text{Fe}^{2+}$  complex translating into an anisotropic relaxation of the primary RP. It is not possible to simulate the  $^3\text{P}$  spectra of *Rps. viridis* RCs measured at  $T \geq 10$  K with the triplet MPS model even with a separate normalization of the amplitudes of the two photoselected spectra. Efforts to calculate the  $^3\text{P}$  line shape of *Rps. viridis* and  $\text{Q}_\text{A}$ -reduced *Rb. sphaeroides* RCs taking into account the spin of the  $\text{Q}_\text{A}^-\text{Fe}^{2+}$  complex are currently underway.

**Nonisotropic Excitation with Unpolarized Light.** There exists a peculiarity of sample excitation, which seems to have evaded until now the attention of EPR spectroscopists who are using sources of unpolarized light for sample excitation. Figure 6a, dots, shows the EPR spectrum of  $^3\text{P}$  in  $\text{Q}_\text{A}$ -reduced RCs of *Rb. sphaeroides* R26 recorded under excitation with depolarized light (Glan-Thompson prism removed). Quite often before, such a spectrum was considered as isotropically excited.<sup>8,10,37</sup> Overlaid on it (Figure 6a, solid line) is the truly isotropic spectrum calculated for equal excitation probability of all RC orientations in the sample. The considerable difference between the two spectra is the result of the nonisotropic character of sample excitation with unpolarized light. This deviation from isotropic excitation arises from the fact that those RCs that are oriented with their primary donor  $\mathbf{Q}_\text{Y}$  moment lying close to parallel to the direction of light propagation have a diminished probability of light absorption. For the molecules with  $\mathbf{Q}_\text{Y}$  exactly parallel to this direction, excitation is zero because the light electric

vector **E**, which is perpendicular to the propagation direction, is then in orthogonal configuration with the transition moment. The calculated truly isotropically excited spectrum agrees very well with a spectrum constructed by summation of one **E**||**B**<sub>0</sub> and two **E**⊥**B**<sub>0</sub> experimental spectra (Figure 6b, dots). In previous publications<sup>8,10,37</sup> the effect of photoselection with unpolarized light was not taken into account. In data treatment, the recorded spectra were considered as isotropic, and the difference between the experimental and the truly isotropically excited spectrum, like that in Figure 6a, was compensated for by varying the kinetic parameters of the triplet sublevels. This resulted<sup>8</sup> in a significant deviation of the **Q**<sub>Y</sub> orientation from the **Q**<sub>Y</sub> angles determined in the present work ( $\delta = 82^\circ$  and  $\gamma = 84^\circ$  were determined for *Rb. sphaeroides* R26 RCs<sup>8</sup>). Photoselection with unpolarized light is partially suppressed by saturating excitation and is weaker in light-scattering samples. This complicates the analysis of the extent of this type of photoselection in the <sup>3</sup>P MPS spectra presented earlier.<sup>8,10,37</sup> The effect of partial photoselection should be taken into account also in the analysis of the light-induced spin-polarized EPR spectrum of the secondary RP (**P**<sup>+</sup>**Q**<sub>A</sub><sup>-</sup>) signals as demonstrated in ref 38. The results of previous simulation attempts<sup>39</sup> should therefore be carefully reconsidered.

## Conclusions

This first DDEPR MPS study of the primary donor triplet states in *Rb. sphaeroides* R26 and *Rps. viridis* reaction centers demonstrates the usefulness of time-resolved EPR for accurately determining orientation parameters. From the simulation of the **E**||**B**<sub>0</sub> and **E**⊥**B**<sub>0</sub> spectra of <sup>3</sup>P, the spherical coordinates of the optical transition moment of the primary donor vs the principal triplet axes were determined with an accuracy of  $\pm 5^\circ$ . The angular parameters are close to those obtained earlier from LD-ADMR measurements. In the 10–50 K temperature range the spherical coordinates are independent of temperature in **Q**<sub>A</sub>-depleted and Zn-substituted *Rb. sphaeroides* R26 preparations. The observed temperature-induced changes of the MPS spectra in nontreated RCs of *Rb. sphaeroides* cannot be described by simple rotation of **Q**<sub>Y</sub>. A much stronger temperature dependence is observed with *Rps. viridis* RCs. Both temperature effects are ascribed to the magnetic interaction between the primary RP **P**<sup>+</sup>**Q**<sub>A</sub><sup>-</sup> and the **Q**<sub>A</sub><sup>-</sup>**Fe**<sup>2+</sup> first acceptor complex, which causes a deviation from the pure **T**<sub>0</sub> population of <sup>3</sup>P.

Since the electric vector of the excitation light is perpendicular to the direction of propagation of the electromagnetic wave, excitation of a sample in an EPR cavity is generally nonisotropic even with unpolarized light. This effect has to be taken into account in simulations of photoinduced magnetically anisotropic states, such as radical pairs, triplet states, etc.

**Acknowledgment.** We thank Ms. S. Jansen for the RC preparations. This work was supported by the Netherlands Foundation for Chemical Research (CW), financed by the Netherlands Organization for Scientific Research (NWO) and by Grant ERBFMRXCT 980214 of the EU TMR program. I.B.K. thanks INTAS (Grant 93-2849-ext) and NWO (Grant 047-003-024) for travel support. I.I.P. acknowledges financial support from FOM (Dutch Foundation for Fundamental Studies of Matter).

## References and Notes

- (1) (a) Deisenhofer, J.; Epp, O.; Miki, K.; Huber, R.; Michel, H. *J. Mol. Biol.* **1984**, *180*, 385. (b) Deisenhofer, J.; Epp, O.; Miki, K.; Huber,

- R.; Michel, H. *Nature* **1985**, *318*, 618. (c) Allen, J. P.; Feher, G.; Yeates, T. O.; Komiya, H.; Rees, D. C. *Proc. Natl. Acad. Sci. U.S.A.* **1987**, *84*, 5730. (d) El-Kabbani, O.; Chang, C.-H.; Tiede, D.; Norris, J.; Schiffer, M. *Biochemistry* **1991**, *30*, 5361.
- (2) Stowell, M. H. B.; McPhillips, T. M.; Rees, D. C.; Soltis, S. M.; Abresch, E.; Feher, G. *Science* **1997**, *276*, 812.
- (3) Hoff, A. J.; Deisenhofer, J. *J. Phys. Rep.* **1997**, *287*, 11.
- (4) Thurnauer, M. C.; Katz, J. J.; Norris, J. R. *Proc. Natl. Acad. Sci. U.S.A.* **1975**, *72*, 3270.
- (5) Budil, D. E.; Thurnauer, M. C. *Biochim. Biophys. Acta* **1991**, *1057*, 1.
- (6) (a) McGlynn S. P.; Azumi, T.; Kinoshita, M. *Molecular Spectroscopy of the Triplet State*; Prentice Hall: Englewood Cliffs, NJ, 1969; Chapter 10. (b) Kottis, P.; Lefebvre, R. *J. Chem. Phys.* **1964**, *41*, 3660. (c) El-Sayed, M. A.; Siegel, S. J. *J. Chem. Phys.* **1966**, *44*, 1416. (d) Lhoste, J.-M.; Haug, A.; Ptak, M. *J. Chem. Phys.* **1966**, *44*, 654. (e) Lhoste, J.-M.; Haug, A.; Ptak, M. *J. Chem. Phys.* **1966**, *44*, 648.
- (7) Thurnauer, M. C.; Norris, J. R. *Biochem. Biophys. Res. Commun.* **1976**, *73*, 501.
- (8) Frank, H. A.; Bolt, J.; Friesner, R.; Sauer, K. *Biochim. Biophys. Acta* **1979**, *547*, 502.
- (9) Boxer, S. G.; Roelofs, M. G. *Proc. Natl. Acad. Sci. U.S.A.* **1979**, *76*, 5636.
- (10) McGann, W. J.; Frank, H. A. *Biochim. Biophys. Acta* **1985**, *807*, 101.
- (11) Bosch, M. K.; Proskuryakov, I. I.; Gast, P.; Hoff, A. J. *J. Phys. Chem.* **1995**, *99*, 15310.
- (12) Rhee, K.; Morris, E. P.; Barber, J.; Kuhlbrandt, W. *Nature* **1998**, *396*, 283.
- (13) (a) Yamauchi, S.; Hirota, N. *J. Chem. Phys.* **1987**, *86*, 5963. (b) Tero-Kubota, S.; Noguchi, T.; Katsuki, A.; Akiyama, K.; Ikegami, Y. *J. Chem. Phys. Lett.* **1991**, *187*, 423. (c) Akiyama, K.; Tero-Kubota, S.; Ikoma, T.; Ikegami, Y. *J. Am. Chem. Soc.* **1994**, *116*, 5324. (d) Regev, A.; Michaeli, S.; Levanon, H.; Cyr, M.; Sessler, J. L. *J. Phys. Chem.* **1991**, *95*, 9121.
- (14) Bosch, M. K.; Proskuryakov, I. I.; Gast, P.; Hoff, A. J. *J. Phys. Chem.* **1996**, *100*, 2384.
- (15) Bosch, M. K. Doctoral Thesis, Leiden University, Leiden, The Netherlands, 1996.
- (16) (a) McLauchlan, K. A. In *Advanced EPR. Applications in Biology and Biochemistry*; Hoff, A. J., Ed.; Elsevier: Amsterdam, 1989; Chapter 10. (b) Stehlik, D.; Bock, C. H.; Thurnauer M. C. *Ibid.*; Chapter 11.
- (17) (a) Proskuryakov, I. I.; Klenina, I. B.; Borovikh, I. V.; Gast, P.; Hoff, A. J. In *Photosynthesis: Mechanisms and Effects*; Garab, G., Ed.; Kluwer: Dordrecht, The Netherlands, 1998; Chapter 24. (b) Klenina, I. B.; Borovikh, I. V.; Gast, P.; Hoff, A. J.; Proskuryakov, I. I. *Dokl. Akad. Nauk* **2000**, *370* (4).
- (18) Feher, G.; Okamura, M. Y. In *The Photosynthetic Bacteria*; Clayton, R. K.; Sistrom, W. R., Eds.; Plenum Press: New York, 1978; Chapter 19.
- (19) Tiede, D. M.; Dutton, P. L. *Biochim. Biophys. Acta* **1981**, *637*, 278.
- (20) Okamura, M. Y.; Isaacson, R. A.; Feher, G. *Proc. Natl. Acad. Sci. U.S.A.* **1975**, *72*, 3491.
- (21) Den Blanken, H. J.; Hoff, A. J. *Biochim. Biophys. Acta* **1982**, *681*, 365.
- (22) Raja, N.; Reddy, S.; Kolaczowski, S. V.; Small, G. J. *J. Phys. Chem.* **1993**, *97*, 6934.
- (23) (a) Kottis, P.; Lefebvre, R. *J. Chem. Phys.* **1963**, *39*, 393. (b) Kottis, P.; Lefebvre, R. *J. Chem. Phys.* **1964**, *41*, 379. (c) Wasserman, E.; Snyder, L.; Yager, W. A. *J. Chem. Phys.* **1964**, *41*, 1763.
- (24) Michl, J.; Thulstrup, E. W. *Spectroscopy with Polarized Light*; VCH Publishers: New York, 1986.
- (25) Vrieze, J.; Hoff, A. J. *Biochim. Biophys. Acta* **1996**, *1276*, 210.
- (26) Hoff, A. J.; Proskuryakov, I. I. *J. Chem. Phys. Lett.* **1985**, *115*, 303.
- (27) Angerhofer, A. In *The Chlorophylls*; Scheer, H., Ed.; CRC Press: Boca Raton, FL, 1991; Chapter 4.
- (28) Lancaster, C. R. D.; Ermler, U.; Michel, H. In *Anoxygenic Photosynthetic Bacteria*; Blankenship, R. E.; Madigan, M. T.; Bauer, C. E., Eds.; Kluwer: Dordrecht, The Netherlands, 1995; Chapter 23.
- (29) Norris, J. R.; Budil, D. E.; Gast, P.; Chang, C.-H.; El-Kabbani, O.; Schiffer, M. *Proc. Natl. Acad. Sci. U.S.A.* **1989**, *86*, 4335.
- (30) Komiya, H.; Yeates, T. O.; Rees, D. C.; Allen, P.; Feher, G. *Proc. Natl. Acad. Sci. U.S.A.* **1988**, *85*, 9012.
- (31) Debus, R. J.; Feher, G.; Okamura, M. Y. *Biochemistry* **1985**, *24*, 2488.
- (32) Van den Brink, J. S.; Manikowski, H.; Gast, P.; Hoff, A. J. *Biochim. Biophys. Acta* **1994**, *1185*, 177.
- (33) Hore, P. J.; Hunter, D. A.; Van Wijk, F. G. H.; Schaafsma, T. J.; Hoff, A. J. *Biochim. Biophys. Acta* **1988**, *936*, 249.

- (34) Wraight, C. A. *FEBS Lett.* **1978**, 93, 283.
- (35) Proskuryakov, I. I.; Manikowski, H. *Dokl. Akad. Nauk SSSR* **1987**, 297, 1250.
- (36) (a) Prince R. C.; Tiede D. M.; Thornber J. P.; Dutton P. L. *Biochim. Biophys. Acta* **1977**, 462, 467. (b) Okamura, M. Y.; Isaacson, R. A.; Feher, G. *Biochim. Biophys. Acta* **1979**, 546, 394.
- (37) Frank, H. A.; Friesner, R.; Nairn, J. A.; Dismukes, G. C.; Sauer, K. *Biochim. Biophys. Acta* **1979**, 547, 484.
- (38) (a) Proskuryakov, I. I.; Klenina, I. B.; Borovykh, I. V.; Gast, P.; Hoff, A. J. *Chem. Phys. Lett.* **1999**, 299, 566. (b) Hulsebosch, R. J.; Borovykh, I. V.; Paschenko, S. V.; Gast, P.; Hoff, A. J. *J. Phys. Chem. B* **1999**, 103, 6815.
- (39) (a) Füchsle, G.; Bittl, R.; Van der Est, A.; Lubitz, W.; Stehlik, D. *Biochim. Biophys. Acta* **1993**, 1142, 23. (b) Van den Brink, J. S.; Hulsebosch, R. J.; Gast, P.; Hore, P. J.; Hoff, A. J. *Biochemistry* **1994**, 33, 13668.